Eur. Phys. J. B **23**, 427–435 (2001)

THE EUROPEAN PHYSICAL JOURNAL B

EDP Sciences

Infrared spectra and lattice vibrations of the spin-chain compound $LiCuVO_4$

B. Gorshunov[1,a], P. Haas[1], M. Dressel[1,b], V.I. Torgashev[2], V.B. Shirokov[2], A.V. Prokofiev[3,c], and W. Assmus[3]

[1] Physikalisches Institut, Universität Stuttgart, Pfaffenwaldring 57, 70550 Stuttgart, Germany
[2] Faculty of Physics, Rostov State University, Zorge Str. 5, 344090 Rostov-on-Don, Russia
[3] Physikalisches Institut, Universität Frankfurt, Robert-Mayer-Str. 2-4, 60054 Frankfurt a.M., Germany

Received 19 February 2001 and Received in final form 26 June 2001

Abstract. The infrared spectra of the one-dimensional antiferromagnet $LiCuVO_4$ are measured in the frequency range from 10 cm^{-1} to 10 000 cm^{-1} and at temperatures from 2 K to 300 K, for the electric field vector **E** of the radiation polarized either along the **a**- or along the **b**-crystallographic directions. For each polarization six infrared active phonon modes are observed in accordance with factor group analysis of the crystal structure of $LiCuVO_4$. The theoretical group analysis of the possible spinel low-symmetry phases is performed within the framework of Landau's theory of phase transitions. The parameters of several phonon lines show noticeable anomalies around 150 K where the magnetic correlations appear in the copper chains, which may indicate a finite interaction between the phonon and the magnon subsystems in $LiCuVO_4$.

PACS. 75.50.Ee Antiferromagnetics – 63.20.Dj Phonon states and bands, normal modes, and phonon dispersion

1 Introduction

Low-dimensional antiferromagnetic systems are attractive for theoretical studies because their magnetic properties can often be described by a simple yet non-trivial Hamiltonian involving only very few parameters. The standard example is the Heisenberg model with only one "free" parameter, the exchange constant J. In spite of being relatively simple, these models allow a number of interesting predictions, like the existence of spinons [1–3]. The field regained attention after the synthesis of inorganic low-dimensional antiferromagnets [4], among them $LiCuVO_4$ [5].

The structure of $LiCuVO_4$ (Fig. 1) contains chains of edge-coupled LiO_6 and CuO_6 octahedra running along the **a**- and **b**-crystal axes, respectively, and can thus be considered to consist of alternatively packed layers each containing arrays of Li^+ or Cu^{2+} chains [6]. The Cu^{2+} ions carry a magnetic moment in this compound. Studies of the magnetic contribution to the susceptibility χ and the magnetic specific heat C_m [7,8] have revealed short-range magnetic correlations which start to play a noticeable role below 150 K, where deviations from the Curie-Weiss like

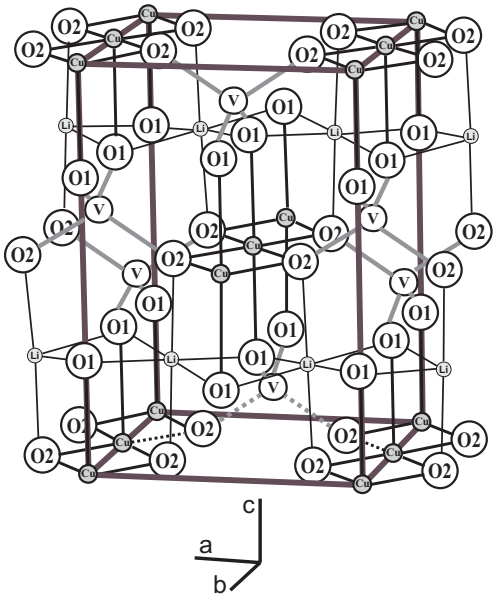

Fig. 1. Orthorhombic unit cell of $LiCuVO_4$. Selected cation-anion bonds are shown by bold lines. The dashed lines show the long-range superexchange interaction between the Cu^{2+} ions forming magnetic chains [12]. The bond lengths are: r(V-O1) = 1.670 Å, r(V-O2) = 1.804 Å, r(Li-O1) = 2.108 Å, r(Li-O2) = 2.185 Å, r(Cu-O1) = 2.409 Å, r(Cu-O2) = 1.970 Å.

[a] *Permanent address*: General Physics Institute, Russian Academy of Sciences, Moscow, Russia
[b] e-mail: dressel@pi1.physik.uni-stuttgart.de
[c] *Permanent address*: A.F. Ioffe Physical Technical Institute, St.-Petersburg, Russia

behavior in the temperature dependence of χ are observed, which result in broad maxima in $\chi(T)$ around 28 K and in $C_{\rm m}(T)$ around 21 K. It has been shown that the temperature behavior of $\chi(T)$ and $C_{\rm m}(T)$ can be well described within the $S = 1/2$ Heisenberg antiferromagnetic linear-chain model [9]. At $T_{\rm N} = 2.4$ K a magnetic phase transition was detected and ascribed to the fact that long-range two-dimensional (2D) ordering of spin chains sets in, showing a dimensional crossover in the magnetic correlations from 1D to 2D (or to 3D [7,8]).

To our knowledge, no optical measurements have been performed on $LiCuVO_4$ so far, which can provide new information on the lattice vibrational modes and on possible interactions between the magnetic, the phonon, and the electronic subsystems. In this paper we report on polarization dependent measurements of the infrared spectra on single crystalline $LiCuVO_4$ performed in the frequency range from 10 cm^{-1} to 10 000 cm^{-1} and in the temperature interval 2 K to 300 K.

2 Experimental details and results

The starting materials for the synthesis of $LiCuVO_4$ were Li_2CO_3(99.9%), V_2O_5(99.5%), and CuO(99.5%). Single crystals of $LiCuVO_4$ were grown by slow cooling of a 40-mol.% solution of $LiCuVO_4$ in a $LiVO_3$ melt. The cooling from 675 to 580 °C was carried out with the rate of 0.5 °C/h. The details have been described earlier [10]. According to X-ray diffraction analysis, the single crystals do not contain inclusions of other phases. For our measurements flat samples of about 5×5 mm^2 with the **a**- and **b**-axes in the sample plane were prepared from the naturally grown crystals. Unfortunately the crystals were too thin (less than a millimeter) to allow us to measure the $\mathbf{E} \parallel \mathbf{c}$ response, *i.e.* the **E** vector of the radiation directed parallel to the **c**-axis.

Reflectivity measurements were performed utilizing a Fourier transform infrared (IR) spectrometer (Bruker IFS 113v) at frequencies $\nu = 30{-}10\,000$ cm^{-1} in the temperature interval from 5 K to 300 K for polarizations $\mathbf{E} \parallel \mathbf{a}$ and $\mathbf{E} \parallel \mathbf{b}$. For these reflectivity measurements the naturally grown sample surface was prepared flat and polished, down to a 0.3 μm diamond powder to avoid light scattering due to surface roughness. The reflection coefficient for each polarization and temperature was determined by normalizing the radiation intensity reflected from the bulk sample to that reflected from a reference mirror (aluminum film on a glass substrate). In addition, a coherent source spectrometer was used for transmission measurements at frequencies 10–23 cm^{-1} and temperatures 2–300 K on an especially prepared plane-parallel slab of a $LiCuVO_4$ crystal with a thickness of *circa* 430 μm (**a**- and **b**-axes in the plane of the slab). From the measured spectra of the transmission coefficient and the phase shift, the real (ε') and the imaginary (ε'') parts of the dielectric constant were determined. The dielectric constant ε' was found to be slightly dependent on temperature. At the frequency of 10 cm^{-1}, for example, we observe a change from $\varepsilon'_a(300\ \mathrm{K}) \approx 11.4$ to $\varepsilon'_a(2\ \mathrm{K}) \approx 10.9$ for the **a**-axis; and for the **b**-axis from $\varepsilon'_b(300\ \mathrm{K}) \approx 10.6$ to $\varepsilon'_b(2\ \mathrm{K}) \approx 10.4$. In this spectral range detailed measurements of the low-temperature behavior of ε' and ε'' did not reveal any anomaly around $T_{\rm N} = 2.4$ K neither in the polarization $\mathbf{E} \parallel \mathbf{a}$ nor $\mathbf{E} \parallel \mathbf{b}$.

Performing a Kramers-Kronig analysis of the IR reflectivity spectra, we obtain the real and imaginary parts of the dielectric constant $\varepsilon'(\nu)$ and $\varepsilon''(\nu)$ of $LiCuVO_4$. The directly measured values of $\varepsilon'(\nu)$ and $\varepsilon''(\nu)$ were utilized to calculate the reflectivity below 30 cm^{-1} as a low-frequency continuation of the correspondent IR data. Frequency independent values of the reflectivity were used as extrapolations towards $\nu = 0$ needed for the Kramers-Kronig analysis; at higher frequencies the standard $R \propto \nu^{-4}$ extrapolations were made.

The reflectivity spectra of $LiCuVO_4$ measured at 5 K and 250 K are presented in Figure 2a and 2b for the two polarizations, $\mathbf{E} \parallel \mathbf{a}$ and $\mathbf{E} \parallel \mathbf{b}$, together with the spectra of the real and imaginary parts of the dielectric constant $\varepsilon'(\nu)$ and $\varepsilon''(\nu)$. Six narrow absorption lines, which obviously are of phonon origin, are clearly seen in the spectra between 100 cm^{-1} and 1000 cm^{-1} for each polarization (note that the highest frequency line for $\mathbf{E} \parallel \mathbf{a}$, although not pronounced in the $\varepsilon'(\nu)$ and $\varepsilon''(\nu)$ spectra, can clearly be distinguished in the reflectivity spectra). Broader peaks are seen above 1000 cm^{-1} and at around 560 cm^{-1} for $\mathbf{E} \parallel \mathbf{a}$ and at 745 cm^{-1} for $\mathbf{E} \parallel \mathbf{b}$; they are shown separately in the insets of Figure 2 where the spectra of ε'' (absorption) are presented with the narrow-lines of the phonon contributions subtracted (according to the analysis described below). We suggest that these broad excitations are due to the response of the electronic subsystem.

To get quantitative information on the parameters of those lines, we have analyzed the dielectric constant and the reflectivity spectra using harmonic oscillator (Lorentzian) terms. Applying a least-mean-square procedure, the spectra of $\varepsilon'(\nu)$ and $\varepsilon''(\nu)$ were fitted by

$$\varepsilon'(\nu) = \varepsilon_{\rm inf} + \sum_i \frac{\Delta\varepsilon_i \nu_i^2 (\nu_i^2 - \nu^2)}{(\nu_i^2 - \nu^2)^2 + \gamma_i^2 \nu^2}, \tag{1}$$

$$\varepsilon''(\nu) = \sum_i \frac{\Delta\varepsilon_i \nu_i^2 \nu\, \gamma_i}{(\nu_i^2 - \nu^2)^2 + \gamma_i^2 \nu^2}\,. \tag{2}$$

Here $\varepsilon_{\rm inf}$ is the high frequency dielectric contribution, ν_i are the eigenfrequency, γ_i the damping, $\Delta\varepsilon_i$ the dielectric contribution with $\Delta\varepsilon_i \nu_i^2$ the oscillator strength of each line. We note that equations (1, 2) do not take into account the electron-phonon interaction which might be present in the spectra since the shape of the absorption lines in the frequency range from 500 cm^{-1} to 1000 cm^{-1} seems to be slightly distorted, probably due to the Fano-resonance effect [11]. Nevertheless in our further analysis we neglect these effects. The obtained parameters of the absorption lines are presented in Table 1 for temperatures 5 K and 250 K; the temperature dependences of the dielectric contribution and the damping are shown in Figure 3 (the eigenfrequencies of all lines were temperature independent within our experimental accuracy, and thus are not shown). The accuracy we achieved with the analysis was

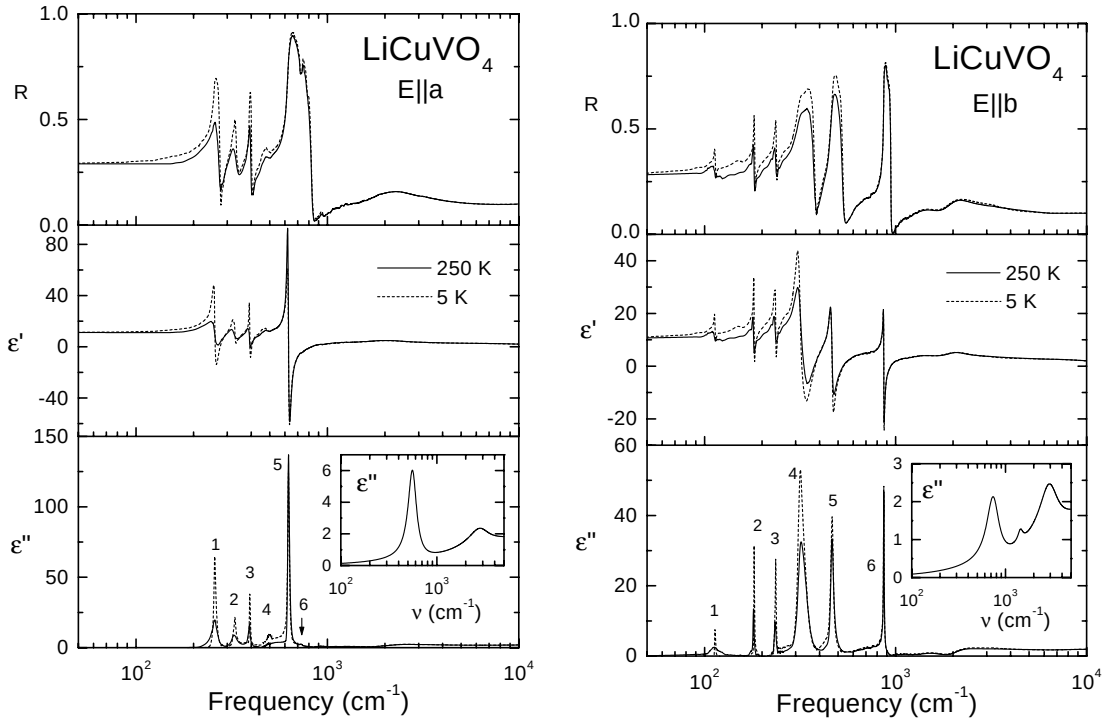

Fig. 2. Spectra of the reflectivity R and of the real ε' and imaginary ε'' parts of the dielectric constant of $LiCuVO_4$ with the electric field polarization $\mathbf{E} \parallel \mathbf{a}$ (a) and $\mathbf{E} \parallel \mathbf{b}$ (b) for two different temperatures $T = 5$ K and 250 K. The phonon lines are numbered as in the Table 1. The insets show the "electronic" absorption spectrum only, with the contribution of the phonon terms to the absorption spectrum $\varepsilon''(\nu)$ subtracted.

Table 1. Parameters of phonon and electronic peaks observed in the infrared spectra of $LiCuVO_4$ single crystal and obtained by a dispersion analysis based on expressions (1) and (2) (see text).

No.	T (K)	$\mathbf{E} \parallel \mathbf{b}$ (B_{2u}-modes)			$\mathbf{E} \parallel \mathbf{a}$ (B_{3u}-modes)		
		ν(cm^{-1})	$\Delta\varepsilon$	γ(cm^{-1})	ν(cm^{-1})	$\Delta\varepsilon$	γ(cm^{-1})
Phonons							
1	5	113	0.08	0.89	259	2.01	9.6
	250	113	0.06	1.70	259	1.14	15.7
2	5	182	0.22	1.27	328	0.74	12.4
	250	182	0.20	2.67	326	0.58	24.1
3	5	236	0.29	2.30	394	0.46	4.92
	250	236	0.21	5.37	393	0.30	7.06
4	5	325	4.1	26.1	486	0.26	35.78
	250	325	3.1	33.3	486	0.18	37.5
5	5	466	1.4	14.9	625	2.65	12.5
	250	466	1.3	22.	625	2.46	12.5
6	5	872	0.65	9.2	733	0.051	23.9
	250	872	0.61	9.7	733	0.035	23.9
Electronic peaks							
7	5	745	0.60	268	560	1.38	137
	250	745	0.63	268	560	0.82	137
8	5	1443	0.05	220	2840	0.574	1628
	250	1443	0.05	220	2840	0.574	1628
9	5	2979	0.68	1616			
	250	2979	0.68	1616			

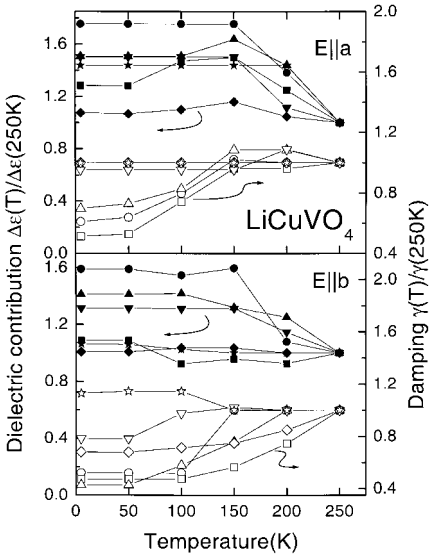

Fig. 3. Temperature dependences of the parameters of the phonon lines in $LiCuVO_4$ obtained by a least square fit of the spectra of reflectivity and real and imaginary parts of the dielectric constant using expressions (1) and (2). The closed symbols denote the dielectric contribution $\Delta\varepsilon$, the open symbols denote the damping constants γ; both $\Delta\varepsilon$ and γ are normalized to their values at 250 K. The lines are numbered as in Figure 2 and Table 1: 1 - circle; 2 - square; 3 - up-triangle; 4 - down-triangle; 5 - diamond; 6 - star.

better than ± 2 cm^{-1} for ν_i and γ_i, and $\pm 10\%$ for $\Delta\varepsilon_i$. In Figure 3 we have normalized the line parameters to their values at 250 K to better visualize their temperature variations.

3 Discussion

3.1 Lattice excitations

The $LiCuVO_4$ structure is an orthorhombically distorted derivative of the cubic spinel structure where the V^{5+} ions are located at the tetrahedral sites and the Li^+ and Cu^{2+} ions are ordered at the octahedral positions [6]. To account for this structure and for the IR phonon modes which we observe in $LiCuVO_4$, we have considered a hypothetical structural phase transformation from a latent phase (Fd3m cubic spinel) to a real Imma structure of $LiCuVO_4$. The room temperature orthorhombic lattice parameters $a = 5.662$ Å, $b = 5.809$ Å and $c = 8.758$ Å [6] indicate that this transformation does not affect the unit cell volume, *i.e.*, it is of a ferrodistorsive (equi-translational) type. As shown in Appendix A, this transformation can be regarded as a phase transition which is composed of ordering (of the Cu^{2+} and Li^+ ions at the position $16(d)$ accompanied by a splitting of the oxygen $32(e)$ position into O1 and O2) and of shifting (of the tetrahedrically coordinated V^{5+} and O^{2-} ions) with the corresponding Jahn-Teller distortions of the CuO_6 octahedra (see also [5]). Following the genesis of this transformation allows us to perform an assignment of the observed phonon lines (see Appendix B). For a cubic spinel the factor-group analysis predicts four IR active vibrational modes while for the Imma structure of $LiCuVO_4$ six optically active phonons are expected to be observed in the IR spectra for each polarization, $\mathbf{E} \parallel \mathbf{a}$ and $\mathbf{E} \parallel \mathbf{b}$. These lines originate from the modes ν_3 (antisymmetric stretching vibration of the V-O bond), ν_4 (deformation vibration of the O-V-O bond), rotation of the tetrahedron R(VO_4), and three translations T(VO_4) + 2T(Li,Cu). Only the lines from the ν_1 and ν_3 modes with the highest frequencies are assigned to VO_4 while the remaining modes are of mixed origin (see Appendix B). In full agreement with our analysis, we experimentally observe six well separated and clearly pronounced resonances for both polarizations (Fig. 2 and Tab. 1). The phonon spectra for $\mathbf{E} \parallel \mathbf{b}$ cover a significantly broader spectral range (113 to 880 cm^{-1}) compared to the $\mathbf{E} \parallel \mathbf{a}$ spectra (260 to 730 cm^{-1}); this difference is caused by the structural anisotropy of the crystal lattice.

We now consider the temperature behavior of the observed phonon lines. As is seen from Table 1, the positions of these lines are practically temperature independent. Only their parameters γ and $\Delta\varepsilon$ for both polarizations change smoothly starting from 250 K down to lower temperatures. Some exceptions are seen in the damping constants for the $\mathbf{E} \parallel \mathbf{a}$ polarization: here the dampings of the three higher frequency lines (number 4, 5 and 6, see Fig. 2a) are temperature independent while a pronounced decrease at around 150 K is observed for the other three lines (number 1, 2 and 3). We do not connect this decrease to the weakening of anharmonic effects because this is expected right below the Debye temperature, which for $LiCuVO_4$ is assumed to be above 300 K, as observed in other spinels (see [22], for example), and also taking into account the observed modes frequencies reaching 800 cm^{-1}. All three lines for $\mathbf{E} \parallel \mathbf{a}$ which show anomalies in $\gamma(T)$ at 150 K originate from bending modes which involve the Cu-O2-V-O2-Cu bonds (see Appendix B). On the other hand, NMR experiments indicate [12] that the strong antiferromagnetic superexchange interaction which is responsible for the one-dimensional antiferromagnetism in $LiCuVO_4$ goes along these Cu-O2-V-O2-Cu paths (see Fig. 1). This interaction is definitely dependent on the correspondent angle since the exchange is determined by an intermediate ion position. This implies that the bending modes essentially participate in the superexchange process. We thus suggest that the observed decrease of the damping constants for modes numbered as 1, 2 and 3 is connected to the finite interaction between the phonon and the magnon subsystems. Since below 150 K the one-dimensional magnetic short-range correlations in the copper chains start to appear and to increase with lowering the temperature [7,13], the spin fluctuations should get weaker and the damping of the bending modes connected with the magnetic subsystem is expected to get smaller.

3.2 Electronic excitations

As far as the observed electronic absorption bands are concerned, we suppose that the peaks found at 2840 cm^{-1} for $\mathbf{E} \parallel \mathbf{a}$ and at 1440 cm^{-1} and 2980 cm^{-1} for $\mathbf{E} \parallel \mathbf{b}$

Table 2. Stable states associated with the irreducible representations $\Gamma_i(\mathbf{k} = 0)$-point of the O_h^7 space group and the corresponding low symmetry phases.

Representation	Equilibrium value of the order-parameter components	Space groups
A_{1g}	η	O_h^7-F4$_1$/d$\bar{3}$2/m
A_{1u}	η	T_h^4-F2/d$\bar{3}$
A_{2g}	η	O^4- F4$_1$32
A_{2u}	η	T_d^2-F$\bar{4}$3m
E_g	η 0	D_{4h}^{19}-I4$_1$/a2/m2/d
	η ξ	D_{2h}^{24}-F2/d2/d2/d
E_u	η 0	D_4^{10}-I4$_1$22
	0 ξ	D_{2d}^9-I$\bar{4}$m2
	η ξ	D_2^7-F222
F_{1g}	η η η	C_{3i}^2-R$\bar{3}$
	0 η η	C_{2h}^3-B2/m
	η 0 0	C_{4h}^6-I4$_1$/a
	η ξ φ	C_i^1-P$\bar{1}$
F_{1u}	η η η	C_{3v}^5-R3m
	0 η η	C_{2v}^{20}-Imm2
	η 0 0	C_{4v}^{11}-I4$_1$md
	η ξ ξ	C_s^3-Bm
	0 η ξ	C_s^4-Bb
	η ξ φ	C_1^1-P1
F_{2g}	η η η	D_{3d}^5-R$\bar{3}$2/m
	η 0 0	D_{2h}^{28}-I2/m2/m2/a
	η ξ ξ	C_{2h}^3- B2/m
	η ξ φ	C_i^1- P$\bar{1}$
F_{2u}	η η η	D_3^7-R32
	0 η η	C_{2v}^{22}-Ima2
	η 0 0	D_{2d}^{12}-I$\bar{4}$2d
	η ξ ξ	C_2^3-B2
	0 η ξ	C_s^4- Bb
	η ξ φ	C_1^1-P1

arise from electronic interband transitions. The peaks at 560 cm^{-1} for $\mathbf{E} \parallel \mathbf{a}$ and at 745 cm^{-1} for $\mathbf{E} \parallel \mathbf{b}$ were introduced in the dispersion analysis in order to describe the correspondent bumps seen in the absorption spectra (see Fig. 2). These peaks can be connected either with the (rather low-energy) interband transitions or with the Fano-like interaction of the phonons with the tails of the electronic peaks at frequencies above 1000 cm^{-1}. For more detailed interpretation, calculations of the electronic excitations spectra are desirable.

4 Conclusions

In conclusion, we have measured the infrared optical properties of single crystalline $LiCuVO_4$ at frequencies between 10 cm^{-1} and 10 000 cm^{-1} in the temperature range from 2 K to 300 K for the electric field vector of radiation polarized along the **a**- and the **b**-crystallographic directions. The theoretical group analysis of the possible spinel low-symmetry phases is performed within the framework of Landau's theory of phase transitions. The possible origin of $LiCuVO_4$ vibrational modes is analyzed. In the experiment, six phonon absorption peaks are observed below 1000 cm^{-1} for each polarization $\mathbf{E} \parallel \mathbf{a}$ and $\mathbf{E} \parallel \mathbf{b}$; this agrees with the factor-group analysis. We find anomalies in the temperature behavior of some lines at around 150 K, where the short range magnetic correlations in the copper chains start to develop. We connect this behavior to an interaction between the phonon and magnon subsystems. In addition, several broad absorption bands have been found above and below 1000 cm^{-1}, presumably of an electronic origin.

The work at Stuttgart was supported by the DFG (Dr 228/14).

Appendix A: Mechanism of a structural transformation from a Fd3m spinel structure to a Imma structure of $LiCuVO_4$

Though $LiCuVO_4$ does not show any real phase transformation up to the melting temperature [5], this structural type can be unambiguously obtained when the order parameter is transformed according to the three-dimensional F_{2g} representation of the Brillouin zone center of the spinel structure, described by the cubic Fd3m symmetry. The ordering behavior in $LiCuVO_4$ was examined by substituting Cu^{2+} for Cu^{3+} ions by lithiation mechanism [5]. The phase transition of an order-disorder type with a distribution of vacancies and cations on the octahedral sites was found in $Li_{2.5}Cu_{0.5}VO_4$. Besides, $LiNiVO_4$ and $LiZnVO_4$ have cubic spinel disordered structures [12] and we can presume a Fd3m $\rightarrow$ Imma phase transition in $Li(Ni_xCu_{1-x})VO_4$ or $Li(Zn_xCu_{1-x})VO_4$. In Table 2 we present the full theoretical group analysis of the structural

Table 3. Vibrational and permutational representations in the Γ point of a cubic spinel structure and selection rules. The numbers show how many times the given irreducible representation is in the permutational representation ($\Gamma_{\rm per}$) or in the vibrational representation ($\Gamma_{\rm vib}$) at the appropriate crystallographic position.

Irreducible representations of O_h point group and selection rules	Wyckoff positions in spinel structure and representations					
	8(a) - T_d		16(d) – D_{3d}		32(e) – C_{3v}	
	$\Gamma_{\rm vibrational}$	$\Gamma_{\rm permutational}$	$\Gamma_{\rm vibrational}$	$\Gamma_{\rm permutational}$	$\Gamma_{\rm vibrational}$	$\Gamma_{\rm permutational}$
A_{1g} (Raman)	-	1	-	1	1	1
A_{1u} (silent)	-	-	-	-	-	-
A_{2g} (silent)	-	-	-	-	-	-
A_{2u} (silent)	-	1	1	-	1	1
E_g (Raman)	-	-	-	-	1	-
E_u (silent)	-	-	1	-	1	-
F_{1g} (rotation)	-	-	-	-	1	-
F_{1u} (IR)	1	-	2	-	2	1
F_{2g} (Raman)	1	-	-	1	2	1
F_{2u} (silent)	-	-	1	-	1	-

phase transitions for the Γ-point of the Brillouin zone for a cubic phase in order to stress the unique choice of the order parameter. Lowering of the symmetry from Fd3m to Imma is accompanied by the appearance of a single non-zero component ($\eta 00$) of the order parameter of the F_{2g} representation [14,15]. The basis vectors of the rhombic and cubic phases of the Bravais cells are connected as:

$$\mathbf{a} = (\mathbf{a}_1 - \mathbf{a}_2)/\sqrt{2}; \quad \mathbf{b} = (\mathbf{a}_1 + \mathbf{a}_2)/\sqrt{2}; \quad \mathbf{c} = \mathbf{a}_3,$$

where $\mathbf{a}$, $\mathbf{b}$, $\mathbf{c}$ and $\mathbf{a}_i$ ($i = 1, 2, 3$) are the basis vectors of the rectangular Bravais cells of the orthorhombic and cubic spinels, respectively. The origin of the low-symmetry cell coordinate system is shifted according to:

$$X_0 = X1_0 + 5/8; \quad Y_0 = Y1_0 + 5/8; \quad Z_0 = Z1_0 + 3/8.$$

The critical F_{2g} mode enters the vibrational representation of the cubic spinel crystal at the 8(a) and 32(e) positions, and it enters the permutational representation at the 16(d) and 32(e) positions; this follows from the factor-group analysis, see Table 3. The mechanism of the ordered orthorhombic modification genesis is determined by the ordering of the Cu^{2+} and Li^{+} ions at the 16(d) position accompanied by a splitting of the oxygen 32(e) position into O1 and O2:

$$8(a) : [V^{5+}] - (Fd3m) = 4(e) : [V^{5+}] - (Imma)$$

$$16(d) : [Cu^{2+}, Li^{+}] - (Fd3m) = 4(a) : [Cu^{2+}] + 4(d) : [Li^{+}] - (Imma)$$

$$32(e) : [O^{2-}] - (Fd3m) = 8(h) : [O1^{2-}] + 8(i) : [O2^{2-}] - (Imma).$$

Besides, this process is accompanied by a shift of the tetrahedrically coordinated V^{5+} and O^{2-} ions. The vanadium cations move only along the z-axis ($z = 0.286c$ in Imma [6]) in opposite directions which causes the cubic cell to stretch along z. The (a) position which was occupied by the vanadium cations in the spinel structure goes to the (e) = $(0, \frac{1}{4}, \frac{3}{8} + \delta_z)$ position, where $\delta_z = 0.011$. The 32(e) position is split into two sublattices: (h) and (i), and in both of them the shift of the (α, α, β) takes place. These sublattices are shifted differently due to the F_{2g} representation which enters twice the $\Gamma_{\rm vibr}$ (Tab. 3). The coordinate of the (h) sublattice, *i.e.*, that of the oxygen O1 [6], equals $(0, -2\delta_x, 1 - \delta_z)$, where $\delta_x = 0.0082$,

$\delta_z = 0.0248$. For the O2 oxygen (i) sublattice coordinates we get: $(1-\delta_x, 1, \delta_z)$, where $\delta_x = 0.0074$ and $\delta_z = 0.0007$.

Appendix B: Vibrational modes assignment in $LiCuVO_4$

For a cubic spinel the factor-group analysis predicts 4 infrared active vibrational modes of the F_{1u} type and 5 Raman active modes: $A_{1g} + E_g + 3F_{2g}$ (see Tab. 3). In many spinel structures these modes were observed experimentally [16–21]. In order to identify the IR active phonons in the orthorhombic phase we correlate the irreducible representations:

Cubic Phase O_h		Orthorhombic Phase D_{2h}
A_{1g}	———	A_g
E_g	———	$A_g + B_{1g}$
F_{1g}	———	$B_{1g} + B_{2g} + B_{3g}$
$3F_{2g}$	———	$3(A_g + B_{2g} + B_{3g})$
$2A_{2u}$	———	$2B_{1u}$
$2E_u$	———	$2(A_u + B_{1u})$
$5F_{1u}$	———	$5(B_{1u} + B_{2u} + B_{3u})$
$2F_{2u}$	———	$2(A_u + B_{2u} + B_{3u})$.

Thus, the IR vibrational spectra of $LiCuVO_4$ must contain $8B_{1u} + 6B_{2u} + 6B_{3u}$ lines (three $B_{1u} + B_{2u} + B_{3u}$ acoustic modes are omitted).

In reference [22] it was proposed to treat the vibrational modes of spinel ferrites of the B_2AX_4 type by considering three individual structural units of a tetrahedral symmetry. In this analysis the 14 atoms per unit cell are grouped into one B_4 tetrahedron and two AX_4 tetrahedra. In $LiCuVO_4$ this grouping leads to one Li_2Cu_2 and two VO_4 units (see Fig. 1). The analysis of the spinel crystal lattice performed in [22] is formally equivalent to a molecular crystal model approach; but in fact the spinel lattice is often regarded (see, for example, [23]) as being intermediate between continuously bonded and molecular-bonded crystals.

In silicate and germanate spinels $(M'_{1-x}M''_x)_2(Si/Ge)O_4(M', M'' = Mg, Ni, Co)$ the infrared spectra depend on the concentration in a complicated manner [17, 18], which indicates that the vibrations of the tetrahedra and octahedra are not independent. This may not only be due to possible interactions of the low-frequency vibrations in the tetrahedral units (VO_4 deformation modes) with the $M'O_6$ and $M''O_6$ vibrations, but due a coupling between these octahedra; thus a simple superpositions of the $M'O_6$ and $M''O_6$ octahedra vibrations will not describe our findings. A similar situation was observed in the superconducting $Li_{1+x}Ti_{2-x}O_4$ spinels [19–21].

We now relate the vibrational representations of the two structural polytypes of $LiCuVO_4$ since it has a spinel structure with ordered octahedral positions. The results are presented in Table 4, together with the symmetrical coordinates. The phonon spectra of $LiCuVO_4$ should contain six IR active absorption lines for both $\mathbf{E} \parallel \mathbf{a}$ (B^x_{3u} modes) and $\mathbf{E} \parallel \mathbf{b}$ (B^y_{2u} modes) polarizations which originate from the modes ν_3 (antisymmetric stretching vibration of the V-O bond), ν_4 (deformation vibration of the O-V-O bond), rotation of the tetrahedron $R(VO_4)$, and three translations $T(VO_4) + 2T(Li,Cu)$. According to the above discussion, we can assume that only the lines from the ν_1 and ν_3 modes with the highest frequencies can be assigned to VO_4; the remaining modes are of mixed origin.

Due to the $O_h^7 \Rightarrow D_{2h}^{28}$ transformation, a Jahn-Teller distortion of the CuO_6 octahedra occurs which is accompanied by the distortion of the adjacent tetrahedron. The ν_3 vibration of the free VO_4^{3-} ion appears in the range 800–825 cm^{-1} [24]. However we expect the degeneracy to be removed, because from the structure analysis of $LiCuVO_4$ we know that the bond lengths r(V-O) in the tetrahedra are distinctly different: $r(V-O1) \approx 1.670$ Å for the bond in the (bc)-plane and $r(V-O2) \approx 1.805$ Å for the bond in the (ac)-plane of the crystal (Fig. 1). Our data confirm this: the position of the antisymmetric V-O1 vibration (short bond) for the $\mathbf{E} \parallel \mathbf{b}$ polarization is at a frequency of 872 cm^{-1} while 624 cm^{-1} (or 733 cm-^{1}) is found for the corresponding mode in the $\mathbf{E} \parallel \mathbf{a}$ polarization. We consider the mode at 624 cm^{-1} rather than the weak line at 733 cm^{-1} to be a B_{3u} component of the ν_3 mode, since the parameters $\Delta\varepsilon$ and γ of the line at 624 cm^{-1} are closer to those of the B_{2u} mode at 872 cm^{-1} (see Tab. 1). A more detailed interpretation of the spectra in the intermediate-frequency region is extremely complicated and beyond the scope of this communication. The bands at 466 cm^{-1} ($\mathbf{E} \parallel \mathbf{b}$) and at 486 cm^{-1} ($\mathbf{E} \parallel \mathbf{a}$) may correspond either to the ν_4 (VO_4^{3-}) bending vibration (which is expected in this region [24]), or to vibrations involving the octahedral cations, or, what is also probable, to complex vibrational modes. The bands with frequencies below 400 cm^{-1} can be assigned to complex vibrations with a predominant contribution of the Li^+ and Cu^{2+} cations.

The reduction of the symmetry due to $O_h^7 \Rightarrow D_{2h}^{28}$ transformation makes two new types of modes to become IR active: the translations of the Li and Cu cations and the vibrations of the VO_4^{3-} tetrahedra of the F_{2u} symmetry (see Tab. 4). While in the cubic spinel selection rules do not allow these modes, in the orthorhombic phase the prohibition is lifted for the B_{2u} and B_{3u} components: two new lines are expected for each polarization $\mathbf{E} \parallel \mathbf{a}$ and $\mathbf{E} \parallel \mathbf{b}$. In the case of $LiCuVO_4$, we assign the lines at 113 cm^{-1} and 230 cm^{-1} for $\mathbf{E} \parallel \mathbf{b}$ and the line at 330 cm^{-1} for $\mathbf{E} \parallel \mathbf{a}$ to these modes. In disordered cubic spinels $LiNiVO_4$ and $LiCoVO_4$ these modes have not been observed yet (see [18]).

Table 4. Correlations of T_d, O_h and D_{2h} irreducible representations and selection rules. Symmetry coordinates are given for cubic spinel phase. Internal modes of vibrations of a T_d tetrahedral group (VO_4) are represented with the usual notation (ν_1 and ν_3 for stretching, ν_2 and ν_4 for bending). The superscript index of representations corresponds to the mode number of atom type. The coordinates of atoms are: Cu_1(5/8 3/8 3/8), Cu_2 (3/8 5/8 3/8), Cu_3 (3/8 3/8 5/8), Cu_4(5/8 5/8 5/8), O_1(3/8,3,8,3/8), O_2(1/8,1,8,3/8), O_3(1/8,3,8,1/8), O_4(3/8,1,8,1/8), V_1(0,0,0), O_5(7/8,7,8,7/8), O_6(1/8,1,8,7/8), O_7(1/8,7,8,1/8), O_8(7/8,1,8,1/8), V_2(1/4,1/4,1/4). Assignments: $W_0 = (x+y+z)$, $W_1 = (x+y-z)$, $W_2 = (x-y+z)$, $W_3 = (-x+y+z)$, $S_0 = (x/2+y/2+z)$, $S_1 = (-x/2-y/2, z)$, $S_2 = (-x/2+y/2-z)$, $S_3 = (x/2-y/2-z)$, $T_1 = (sx+sy+0)$, $T_2 = (sx-sy+0)$, $s = \sqrt{3}/2$.

Irreducible representations of the T_d group		First tetrahedron					Second tetrahedron					Cu - sublattice				Irreducible representations	
		O_1	O_2	O_3	O_4	V_1	O_5	O_6	O_7	O_8	V_2	Cu_1	Cu_2	Cu_3	Cu_4	O_h^7	
		O_1^1	O_2^1	O_2^2	O_1^2	V_1	O_4^1	O_3^1	O_3^2	O_4^2	V_2	Li_1	Li_2	Cu_1	Cu_2		D_{2h}^{28}
$A_1^{(O)}$	ν_1	W_0	$-W_1$	$-W_2$	$-W_{3'}$		W_0	$-W_1$	$-W_2$	$-W_{3'}$						$A_{2u}^{(O)}$	B_{1u}^1
$E^{(O)}$	ν_2	S_1 T_2	S_0 $-T_2$	S_3 $-T_1$	S_2 T_1		S_1 T_2	S_0 $-T_2$	S_3 $-T_1$	S_2 T_1						$E_u^{(O)}$	B_{1u}^2 A_u^1
$F_1^{(O)}$	R	y-z -x-z x-y	y+z -x+z -x-y	-y+z x-z x+y	-y-z x+z -x+y		y-z -x-z x-y	y+z -x+z -x-y	-y+z x-z x+y	-y-z x+z $-V_3$						$F_{2u}^{(O)}$	$B_{2u}^1+B_{3u}^1$ A_u^2
$F_2^{1(O)}+F_2^{(V)}$	T	x y z	x y z	x y z	x y z	x y z	x y z	x y z	x y z	x y z	x y z	x y z	x y z	x y z	x y z	$F_{1u}^{1(O)}$ $+F_{1u}^{(V)}$ $+F_{1u}^{1(Cu)}$	$B_{2u}^2+B_{3u}^2$ B_{1u}^3
$F_2^{1(O)}-F_2^{(V)}$	ν_3	x y z	x y z	x y z	x y z	-x -y -z	x y z	x y z	x y z	x y z	-x -y -z					$F_{1u}^{1(O)}-F_{1u}^{(V)}$	$B_{2u}^3+B_{3u}^3$ B_{1u}^4
$F_2^{2(O)}$	ν_4	y+z x+z x+y	y-z x-z -x+y	-y-z -x+z x-y	-y+z -x-z -x-y		y+z x+z x+y	y-z x-z -x+y	-y-z -x+z x-y	-y+z -x-z -x-y						$F_{1u}^{2(O)}$	$B_{2u}^4+B_{3u}^4$ B_{1u}^5
-	-											x y z	x y z	x y z	x y z	$F_{1u}^{1(Cu)}$	$B_{2u}^5+B_{3u}^5$ B_{1u}^6
-	-											y+z x-z x-y	y-z x+z -x-y	-y-z -x-z x+y	-y+z -x+z -x+y	$F_{1u}^{2(Cu)}$	$B_{2u}^6+B_{3u}^6$ B_{1u}^7
-	-											y-z -x+z x+y	y+z -x-z -x+y	-y+z x+z x-y	-y-z x-z -x-y	$F_{2u}^{(Cu)}$	$B_{2u}^7+B_{3u}^7$ A_u^3
$A_1^{(O)}$	ν_1	W_0	$-W_1$	$-W_2$	$-W_{3'}$		$-W_0$	W_1	W_2	$W_{3'}$						$A_{1g}^{(O)}$	A_g^1
$E^{(O)}$	ν_2	S_1 T_2	S_0 $-T_2$	S_3 $-T_1$	S_2 T_1		$-S_1$ $-T_2$	$-S_0$ T_2	$-S_3$ T_1	$-S_2$ $-T_1$						$E_g^{(O)}$	A_g^2 B_{1g}^1
$F_1^{(O)}$	R	y-z -x-z x-y	y+z -x+z -x-y	-y+z x-z x+y	-y-z x+z -x+y		-y-z x-z -x-y	-y+z x+z x-y	y+z -x-z -x+y	y-z -x+z x+y						$F_{1g}^{(O)}$	$B_{2g}^1+B_{3g}^1$ B_{1g}^2
$F_2^{1(O)}+F_2^{(V)}$	T	x y z	x y z	x y z	x y z	x y z	-x -y -z	-x -y -z	-x -y -z	-x -y -z	-x -y -z					$F_{2g}^{1(O)}+F_{2g}^{(V)}$	$B_{2g}^2+B_{3g}^2$ A_g^3
$F_2^{1(O)}-F_2^{(V)}$	ν_3	x y z	x y z	x y z	x y z	-x -y -z	-x -y -z	-x -y -z	-x -y -z	-x -y -z	x y z					$F_{2g}^{1(O)}-F_{2g}^{(V)}$	$B_{2g}^3+B_{3g}^3$ A_g^4
$F_2^{2(O)}$	ν_4	y+z x+z x+y	y-z x-z -x+y	-y-z -x+z x-y	-y+z -x-z -x-y		-y+z -x+z -x+y	-y-z -x-z x+y	y-z x+z -x-y	y+z x-z x-y						$F_{2g}^{2(O)}$	$B_{2g}^4+B_{3g}^4$ A_g^5
-	-											$-W_3$	$-W_2$	$-W_1$	$W_{0'}$	$A_{2u}^{(Cu)}$	B_{1u}^8
-	-											T_1 S_3	$-T_1$ S_2	$-T_2$ S_1	T_2 S_0	$E_u^{(Cu)}$	B_{1u}^9 A_u^4

References

1. L.D. Faddeev, L.A. Takhtajan, Phys. Lett. A **85**, 375 (1981).
2. D.A. Tennant, R.A. Cowley, S.E. Nagler, A.M. Tsvelik, Phys. Rev. B **52**, 13368 (1995).
3. O.V. Misochko, S. Tajima, C. Urano, H. Eisaki, S. Uchida, Phys. Rev. B **53**, R14733 (1996).
4. E. Dagotto, Rep. Prog. Phys. **63**, 1525 (1999).
5. R. Kanno, Y. Kawamoto, Y. Takeda, M. Hasegawa, O. Yamamoto, N. Kinomura, J. Solid State Chem. **96**, 397 (1992); R. Kanno, Y. Kawamoto, Y. Takeda, M. Hasegawa, O. Yamamoto, Solid State Ionics **40/41**, 576 (1990).
6. M.A. Lafontaine, M. Leblanc, G. Ferey, Acta Cryst. C **45**, 1205 (1989).

7. M. Yamaguchi, T. Furuta, M. Ishikawa, J. Phys. Soc. Jpn **65**, 2998 (1996).
8. A.N. Vasil'ev, JETP Letters **69**, 876 (1999).
9. J.C. Bonner, M.E. Fisher, Phys. Rev. **135**, A640 (1964).
10. A.V. Prokofiev, D. Wichert, W. Assmus, J. Cryst. Growth **220**, 345 (2000).
11. U. Fano, Phys. Rev. **124**, 1866 (1961).
12. H. Saji, J. Phys. Soc. Jpn **33**, 671 (1972).
13. R.B. Griffiths, Phys. Rev. Lett. **23**, 17 (1969).
14. V.P. Sakhnenko, V.M. Talanov, G.M. Chechin, Fizika Metallov I Metallovedenie (in Russian) **62**, 847 (1986).
15. C.J. Haas, J. Phys. Chem. Sol. **26**, 1225 (1965).
16. P.F. McMillan, A.M. Hofmeister, Reviews Mineral **18**, 99 (1988).
17. P. Tarte, Mem. Acad. Roy. Belgique **35**, 260 (1965).
18. J. Preudhomme, P. Tarte, Spectrochim. Acta, A **28**, 69 (1972).
19. T. Oda, M. Shirai, N. Suzuki, K. Motizuki, J. Phys. Cond. Matt. **6**, 6997 (1994).
20. M.A. Green, M. Dalton, K. Prassides, P. Day, D.A. Neumann, J. Phys. Cond. Matt. **9**, 10855 (1997).
21. F. Compf, B. Renker, H. Mutka, Physica B **180-181**, 459 (1992).
22. R.D. Waldron, Phys. Rev. **99**, 1727 (1955).
23. W.B. White, B.A. DeAngelis, Spectrochim. Acta, A **23**, 985 (1967).
24. K. Nakamoto, *Infrared and Raman Spectra of Inorganic and Coordination Compounds*, 4th edn. (Wiley-Interscience, New York, 1986); W. Zeil, R. Dautel, W.Z. Honsberg, Elektrochem. **60**, 1131 (1956).